PHYSICAL REVIEW B **88**, 140507(R) (2013)

Superconductivity in $Ba_{n+2}Ir_{4n}Ge_{12n+4}$ ($n = 1,2$) with cage structure and softening of low-lying localized mode

Jiangang Guo,[1] Jun-ichi Yamaura,[2] Hechang Lei,[1] Satoru Matsuishi,[2] Yanpeng Qi,[1] and Hideo Hosono[1,2,3,*]

[1]*Frontier Research Center, Tokyo Institute of Technology, Yokohama 226-8503, Japan*

[2]*Materials Research Center for Element Strategy, Tokyo Institute of Technology, Yokohama 226-8503, Japan*

[3]*Materials and Structures Laboratory, Tokyo Institute of Technology, Yokohama 226-8503, Japan*

(Received 17 August 2013; published 23 October 2013)

We report on new superconductors $Ba_{n+2}Ir_{4n}Ge_{12n+4}$ (n = 1, 2) with critical temperatures T_c = 6.1 and 3.2 K, respectively, along with their crystal structures, electron transport, and specific heat. The compounds are composed of alternating $Ba@Ir_8Ge_{16}$ and $Ba@Ir_2Ge_{16}$ cages, both of which are larger in the $n = 1$ sample than in the $n = 2$ sample. The normal-state heat capacity reveals two low-lying vibration modes associated with guest Ba cations, and both characteristic temperatures in $Ba_3Ir_4Ge_{16}$ are smaller than those in $Ba_4Ir_8Ge_{28}$. Meanwhile, the density functional theory calculations reveal that the Ge-4p bands dominated the Fermi level in both samples. We propose that the softening of localized phonons due to expansion of the cage strengthens the electron-phonon coupling between Ba cations and Ge anions, leading to the higher T_c in $Ba_3Ir_4Ge_{16}$.

DOI: 10.1103/PhysRevB.88.140507 PACS number(s): 74.81.Bd, 74.25.Bt, 74.25.Ld, 74.25.Jb

I. INTRODUCTION

The weakly bound nature of guest atoms encapsulated in a cage structure could induce a low-energy, anharmonic vibration, which has significant influence on lattice dynamics and electron-phonon coupling (λ_{e-ph}).[1] Such a distinct eigenmode of the guest atoms, which is called as the rattling, was evidenced in well-known filled skutterudites,[2] coupled with acoustic phonons to reduce the thermal conductivity in favor of high-performance thermoelectric materials.[3] The superconductivity mediated by the rattling in structures like clathrates,[4] filled skutterudites,[5] and Chevrel-phase compounds[6] remains elusive; likewise, a clear correlation between low-energy vibration and critical temperature (T_c) has not been established.

Recently, superconductivity was discovered in the classic Einstein solid A_xVAl_{10} (A = Al, Ga), where the local vibration due to rattling of the A atom couples with the low-frequency phonons and conductive electrons in favor of superconductivity.[7,8] In addition, in β-pyrochlore AOs_2O_6 (A = K, Rb, Cs) superconductors,[9] the low-lying excitation state from the rattling guest atom in the OsO_6 cage can be systemically tuned by changing the size of encapsulated atoms.[10,11] That is, the rattling magnitude of the A atom increases as its size decreases, as evidenced by the largest value of the isotropic temperature factor (U_{iso}) for the K ion.[12] The weakened bonding states between the A atoms and the cage wall lead to lowering of the Einstein temperature and characteristic energy. It has been proposed that the softening of low-lying modes, coupled with the acoustic phonons of the cage, results in enhanced λ_{e-ph} and the highest measured T_c for KOs_2O_6.[13]

There should be other approaches, such as tuning the size and weight of the framework in cage compounds, to control the λ_{e-ph} strength and T_c. In this Rapid Communication, we report on two new cage superconductors, $Ba_{n+2}Ir_{4n}Ge_{12n+4}$ ($n = 1, 2$), with $T_c = 6.1$ and 3.2 K, respectively. The structures are composed of the layers made of Ir-Ge cages, that is, those with noncubic crystal symmetry, in marked contrast to the rattling compound previously documented. The analysis of normal-state heat capacity demonstrated low-lying vibration modes arising from the motion of capsulated Ba cations. The Debye and characteristic Einstein temperatures decrease as the scale of the cage increases. Higher T_c in $Ba_3Ir_4Ge_{16}$ is discussed in terms of enhanced λ_{e-ph} due to the reduction of the average phonon spectrum ($\langle\omega^2\rangle$) and low-energy phonon softening involving looser bonds between the guest atoms and the cage wall.

II. EXPERIMENTAL DETAILS

Polycrystalline samples of $Ba_3Ir_4Ge_{16}$ were synthesized by arc melting and subsequent annealing at 1073 and 1273 K for 10 h, respectively. A single crystal of $Ba_4Ir_8Ge_{28}$ was grown by the IrGe-flux method; i.e., the mixture was heated to 1373 K, cooled down to 1173 K at a rate of 4 K/h, and finally furnace cooled to room temperature. The powder x-ray diffraction (PXRD) pattern of $Ba_3Ir_4Ge_{16}$ was collected using a Bruker diffractometer model D8 Advance (Cu rotating anode). Rietveld refinement of the PXRD patterns was performed using TOPAS version 3 code.[14] Oscillation photographs of $Ba_4Ir_8Ge_{28}$ single crystals were taken at room temperature using a curved imaging plate (Rigaku R-Axis Rapid-II). Monochromatic Mo-Kα radiation generated by a rotating anode with a confocal mirror (Rigaku VariMax) was used as an x-ray source. Data integration and absorption correction were performed with Rapid-Auto. Structural parameters were refined by the full-matrix least-squares method using the Crystal Structure program package. The chemical compositions of the samples were determined by electron probe microscope analysis with the backscattered electron mode. The electrical resistivity (ρ) and specific heat capacity (C_p) were measured through the standard four-wire method and through the thermal relaxation method using the physical property measurement system (Quantum Design), respectively. The dc magnetic properties were characterized using a vibrating sample magnetometer (SVSM, Quantum Design).

Density functional theory (DFT) calculations were performed using the generalized gradient approximation with the Perdew-Burke-Ernzerhof function and the projected

augmented plane-wave method implemented in the Vienna *Ab initio* Simulation Package.[15] A triclinic primitive cell ($a = b \sim 6.6$ Å, $c \sim 12.2$ Å; $\alpha = \beta \sim 106^\circ$; $\gamma = 90.0^\circ$) for $n = 1$ and an orthorhombic conventional cell ($a \approx 38.3$ Å, $b \approx 6.50$ Å, $c \approx 6.53$ Å) for $n = 2$ were used for the calculation and the lattice parameters, and atomic positions were fully relaxed by a structural optimization procedure minimizing the total energy and force. Self-consistent solutions of the Kohn-Sham equations were obtained by employing $4 \times 4 \times 2$ and $1 \times 4 \times 4$ Monkhorst-Pack grids of k points for integration over the Brillouin zone for $n = 1$ and 2, respectively. The plane-wave basis-set cutoff was set to 500 eV. The full electronic density of states (DOS) was also calculated with high k-point samplings of $8 \times 8 \times 4$ and $2 \times 8 \times 8$. The projected DOS of each atom was obtained by decomposing the charge density over the atom-centered spherical harmonics.

III. RESULTS AND DISCUSSION

A. Crystal structure

Figure 1 shows the crystal structures of $Ba_3Ir_4Ge_{16}$ and $Ba_4Ir_8Ge_{28}$. The crystal structure of $Ba_3Ir_4Ge_{16}$ was refined as an analogous $Ba_3Rh_4Ge_{16}$ structural model.[16] The obtained crystal structure of $Ba_3Ir_4Ge_{16}$ ($n = 1$) has a tetragonal lattice (space group, $I4/mmm$) with $a = 6.5387(4)$ Å and $c = 22.2834(4)$ Å. The crystal structure for $Ba_4Ir_8Ge_{28}$ ($n = 2$) has an orthorhombic lattice (space group, *Pmna*) with $a = 37.737(4)$ Å, $b = 6.4246(6)$ Å, and $c = 6.4567(6)$ Å. The results of the structural refinements are summarized in the Supplemental Material.[17] In both crystal structures, the

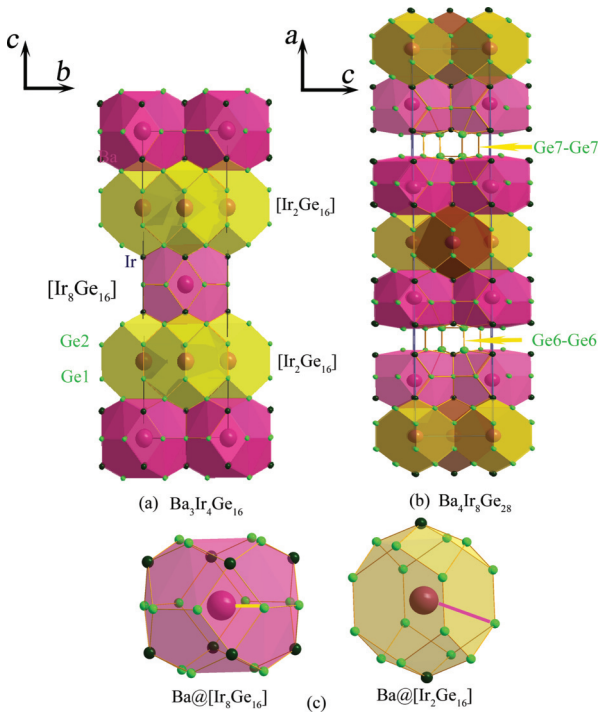

FIG. 1. (Color online) Crystal structure. The crystal structures of (a) $Ba_3Ir_4Ge_{16}$ and (b) $Ba_4Ir_8Ge_{28}$. The short Ge-Ge covalent bonds between $[Ir_8Ge_{16}]$ cages are labeled. (c) The local structures of Ba@$[Ir_8Ge_{16}]$ and Ba@$[Ir_2Ge_{16}]$ cages. The shortest distance between Ba and Ge is highlighted in each cage.

$[Ir_8Ge_{16}]^{2-}$ cages are connected by $[Ir_2Ge_{16}]^{2-}$ cages encapsulating barium atoms. Specifically, the crystal structure of $Ba_3Ir_4Ge_{16}$ has alternating Ba@$[Ir_2Ge_{16}]$ and $BaIr_4Ge_{12}$ layers made of face-shared Ba@$[Ir_8Ge_{16}]$ cages. In $Ba_4Ir_8Ge_{28}$, there are subunits formed by two layers of Ba@$[Ir_8Ge_{16}]$ cages, which are intraconnected by the crossed Ge-Ge bond and are sandwiched by two types of Ba@$[Ir_2Ge_{16}]$ cages. In both compounds, the shortest Ge_1-Ge_2 distance is ~2.45 Å, which is approximately equivalent to that of cubic Ge and is indicative of a strong covalent bond.[18] The bond lengths of Ge_6-Ge_6 and Ge_7-Ge_7 were 2.623(3) and 2.564(4) Å, respectively, each of which is shorter than the Ge-Ge separation in the cage wall. In Fig. 1(c), we show the coordination of the Ba@$[Ir_8Ge_{16}]$ and Ba@$[Ir_2Ge_{16}]$ cages. At $n = 2$, the shortest distances between Ba and Ge ions are 3.506(2) and 3.452(1) Å in the above two cages, respectively. The counterparts for $n = 1$ increase to 3.596(8) and 3.495(2) Å in the above two cages, respectively. This enhanced space for Ba cations could possibly weaken the bond between Ba and the cage wall and thus reduce the rattling frequency of the Ba cations.

B. Electron transport and low-temperature heat capacity

Figure 2 shows the temperature dependence of electrical resistivity for $Ba_{n+2}Ir_{4n}Ge_{12n+4}$ ($n = 1$, 2). Both compounds exhibit typically metallic behavior. The concave-downward behaviors of $\rho(T)$ curves are shown in Figs. 2(a) and 2(c), indicating that electron-phonon scattering is dominant in the high-temperature region. A similar trend of resistivity has been observed in other cagelike superconductors, such as skutterudites[19] and β-pyrochlore oxides.[5] This observation is attributed to the strong electron-phonon scattering due to the anharmonic rattling of guest atoms in the oversized cage. Both $\rho(T)$ data could be well described by the phonon-assisted Bloch-Grüneisen formula:

$$\frac{1}{\rho(T)} = \frac{1}{\rho_i} + \frac{1}{\rho_s} \tag{1}$$

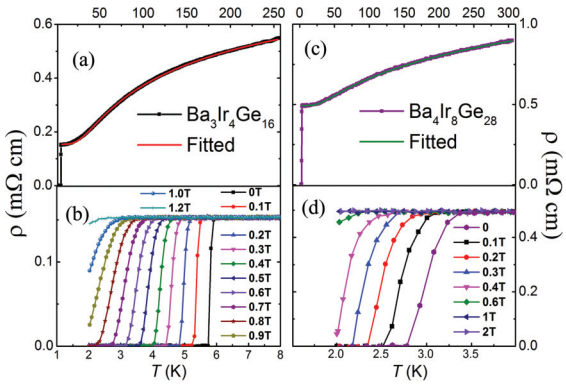

FIG. 2. (Color online) Electronic transport and magnetic properties. The temperature dependences of electrical resistivity for the (a) $Ba_3Ir_4Ge_{16}$ and (c) $Ba_4Ir_8Ge_{28}$ samples under zero magnetic field. The solid lines represent the fitting results for the Bloch-Grüneisen model. The electrical resistivity of the (b) $Ba_3Ir_4Ge_{16}$ and (d) $Ba_4Ir_8Ge_{28}$ samples measured in a lower temperature range at a magnetic field up to 20 kOe.

$$\rho_s = \frac{v_F}{\varepsilon_0 \Omega_p^2 a} \quad (2)$$

$$\rho_i(T) = \rho(0) + A\left(\frac{T}{\Theta_D^*}\right)^5 \int_0^{\frac{\Theta_D^*}{T}} \frac{x^5}{(e^x - 1)(1 - e^{-x})} dx \quad (3)$$

where $\rho(0)$ is the residual resistivity, v_F is the Fermi velocity, Ω_p is the plasma frequency, a is the interatomic spacing, $\Theta_D{}^*$ is the Debye temperature, and A is a constant depending on the material. The fitting results of $\rho(T)$ yield $\Theta_D{}^* = 171(2)$ and 240(4) K for $Ba_3Ir_4Ge_{16}$ and $Ba_4Ir_8Ge_{28}$, respectively. At low temperatures of normal-state ρ, the resistivity is found to vary with the T^2 dependence, which means the electron-electron scattering is important. As shown in Fig. 2(b) and 2(d), the electrical resistivity suddenly drops to zero due to superconducting transitions at $T_c{}^{\text{onset}} = 6.1$ and 3.2 K for $Ba_3Ir_4Ge_{16}$ and $Ba_4Ir_8Ge_{28}$, respectively. The superconducting transition is gradually suppressed by the magnetic field. The upper critical field $H_{c2}(0)$, as shown in Fig. 3(a), can be determined by Werthammer-Helfand-Hohenberg (WHH) theory as the criterion of 90% of the normal resistivity at various fields. Based on the calculated $H_{c2}(0) = 18.2(2)$ and 16.3(4) kOe, we can estimate the Ginzburg-Landau coherence lengths $\xi = 134.5(5)$ and 142.1(3) Å for $Ba_3Ir_4Ge_{16}$ and $Ba_4Ir_8Ge_{28}$, respectively.

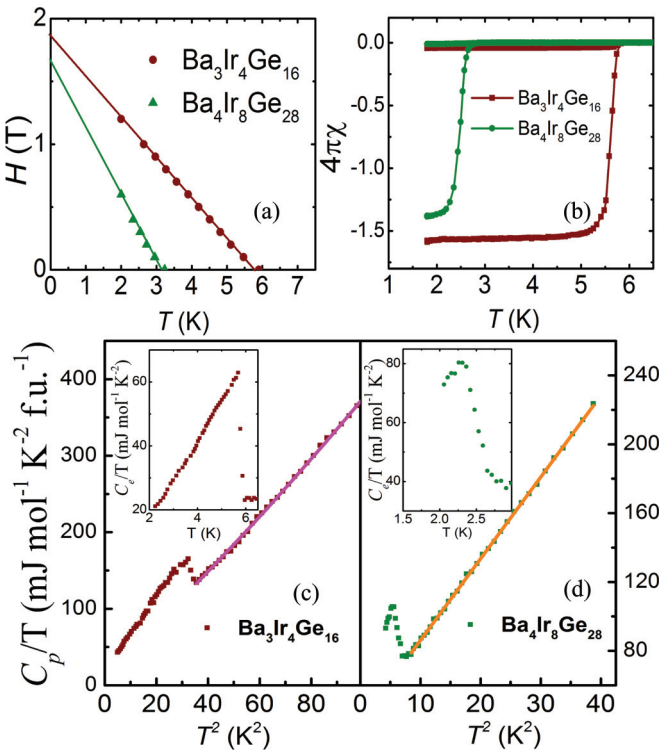

FIG. 3. (Color online) Superconducting properties. (a) The upper critical field $H_{c2}(0)$ obtained from 90% resistivity data following WHH theory. (b) The superconducting volume fraction for $Ba_3Ir_4Ge_{16}$ and $Ba_4Ir_8Ge_{28}$ as a function of temperature. The specific heat data of (c) $Ba_3Ir_4Ge_{16}$ and (d) $Ba_4Ir_8Ge_{28}$ samples in the vicinity of the superconducting transition. The solid lines are fitting results with the Debye model, combined with the high-frequency phonon part. Each inset shows the jump of the electronic part of the heat capacity around T_c.

In Fig. 3(b), the bulk superconductivity was further confirmed by the magnetization at low temperatures. Large diamagnetic signals were observed for both compounds. The hysteresis between zero-field-cooling and field-cooling curves clearly indicates these two compounds are type-II superconductors. The normal-state susceptibilities come almost from core diamagnetism, and no magnetic phase transition occurs in the range of 5 to 300 K. The low-temperature upturns imply that the samples may contain a small amount of paramagnetic impurity.[17] Figure 3(c) and 3(d) shows the curves of C_p/T versus T^2 at the low-temperature zone for $n = 1$ and 2 samples, respectively. A combination of the Debye model and the high-energy phonon contribution, $C_p/T = \gamma + \beta T^2 + \eta T^4$, was better to fit the data, which may due to the abnormal dispersion of phonon spectrum in such a complex crystal structure. For $n = 1$ and 2, respectively, the Sommerfeld coefficient γ was found to be 21(2) and 36(3) mJ mol^{-1} K^{-2} $f.u.^{-1}$ and the Debye temperature $\Theta_{D'}$ was found to be 240(3) and 254(2) K. Meanwhile, the normalized specific heat jump $\Delta C_e/\gamma T_c$ of $Ba_3Ir_4Ge_{16}$, 1.85, was obviously greater than the value of $Ba_4Ir_8Ge_{28}$ (1.31) and the Bardeen-Cooper-Schrieffer (BCS) weak-coupling limitation (1.43), as shown in the inset of Fig. 3(b). In addition, the unexpectedly large γ value of $Ba_4Ir_8Ge_{28}$ was confirmed by our DFT calculations.[17] From Fig. 4(a) and 4(b), we can see that the contribution of Ge $4p$ states dominated the Fermi level, and the Ge $4p$-like states slightly hybridized with the Ir $5d$ orbital around the Fermi level. The Fermi level is located between the bonding (σ) state and the antibonding (σ^*) state of the Ge-Ge bond, and the electrons from Ge dominate the conductivity. From the total DOS value at the Fermi level, we can obtain the theoretical Sommerfeld coefficient (γ^*) of both compounds to be 31.1 and 66.2 mJ mol^{-1} K^{-2} $f.u.^{-1}$ for $n = 1$ and 2, respectively. It was found that variation of neither γ nor γ^* was proportional to the magnitude of T_c according to BCS theory. Simultaneously, the calculated γ_{atom} is 0.91(1) and 0.90(1) mJ mol^{-1} K^{-2} $atom^{-1}$ for $n = 1$ and 2; the nearly identical electron contribution implies that the λ_{e-ph} strength may be more important in accounting for the scale of T_c.

C. Normal-state thermal property

Taking into account the expansion of $[Ir_8Ge_{16}]$ and $[Ir_2Ge_{16}]$ cages in $Ba_3Ir_4Ge_{16}$, it recalls that the smallest ions (K^+) in the OsO_6 cage induce the strongest λ_{e-ph} and the highest T_c among β-pyrochlore superconductors.[13] It is natural to examine the variation of low-lying local modes arising from the rattling of Ba atoms, which possibly affects the scale of T_c. Figure 4(c) and 4(d) shows the normal-state specific heat data of $Ba_{n+2}Ir_{4n}Ge_{12n+4}$ ($n = 0$, 1, 2). As we can see, broad peaks emerge ~20 K for two caged samples, which manifest the presence of a low-energy Einstein vibration like the vibration of alkalis/alkaline-earth metals in canonical glass and clathrates.[20] This so-called boson peak always involves the local vibration modes[21] or anomaly in the transverse acoustic phonon.[22] In contrast, the absence of an isolated peak in $BaGe_2$ ($n = 0$) demonstrates the significance of the Ba atom rattling in its cage and can be well produced by a single Debye model. Regarding the $n = 1$ and 2 samples, we used the sum of the

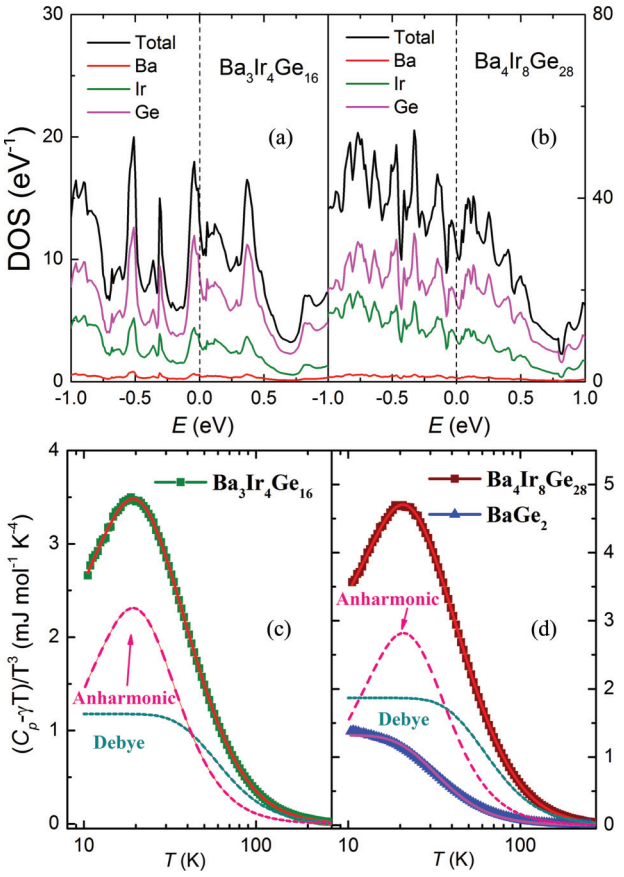

FIG. 4. (Color online) Electronic structure and analysis of the localized phonon modes. The DOS around the Fermi level for (a) $Ba_3Ir_4Ge_{16}$ and (b) $Ba_4Ir_8Ge_{28}$. The Fermi energy is set as zero energy. (c) and (d) The normal-state specific heat data of $Ba_{n+2}Ir_{4n}Ge_{12n+4}$ (n = 0, 1, 2) are plotted in the form of $(C_p - \gamma T)/T^3$ vs T. The solid lines are the fitting curves discussed in text. The dashed lines are the individual contributions of Debye and Einstein parts.

Debye model and Einstein oscillators to the fit the data of the two cage superconductors,

$$C_p - \gamma T = C_D + C_E \tag{4}$$

$$C_D = 9N_dR\left(\frac{T}{\Theta_D}\right)^3 \int_0^{\Theta_D/T} \frac{\zeta^4 e^\zeta}{(e^\zeta - 1)^2} d\zeta;$$

$$C_E = C_{E_1} + C_{E2}$$

$$= 3N_1R\left(\frac{\Theta_E}{T}\right)^2 \frac{e^{\frac{\Theta_E}{T}}}{\left(e^{\frac{\Theta_E}{T}} - 1\right)^2} + 3N_2R\left(\frac{\Theta_E}{T}\right)^2 \frac{e^{\frac{\Theta_E}{T}}}{\left(e^{\frac{\Theta_E}{T}} - 1\right)^2} \tag{5}$$

where C_D and C_E are the contributions of rigid Ir-Ge cage and the rattling Ba cations, respectively; N_d is 20 and 36 per mole for $n = 1$ and 2, respectively; N_1 and N_2 are the numbers of oscillators per formula; R is the gas constant; and Θ_D and Θ_E are the Debye and Einstein temperatures, respectively. The converged fitting gave $\Theta_D = 286(4)$ K, $\Theta_{E1} = 113(1)$ K, and $\Theta_{E2} = 53(1)$ K for $n = 1$ and $\Theta_D = 303(3)$ K, $\Theta_{E1} = 118(1)$ K, and $\Theta_{E2} = 60(1)$ for $n = 2$. The obtained Debye and Einstein temperatures were comparable to counterparts of β-pyrochlore and skutterudite superconductors[13,19] and insensitive to the selected temperature range (shown in Table I), suggesting the reasonable fitting procedure. Furthermore, the Debye and Einstein temperatures of $Ba_3Ir_4Ge_{16}$ were smaller than those of $Ba_4Ir_8Ge_{28}$, implying that there may be phonon softening due to the decreased motion frequency of rattlers in the expanded cage.

D. Phonon softening and superconductivity

Next, we qualitatively discuss the influence of phonon softening on the magnitude of T_c. The λ_{e-ph} constants of both compounds could be calculated using the Macmillan equation with the observed T_c and Θ_D.[17] Summarized parameters are listed in Table I. We can see that the λ_{e-ph} strength increases from 0.56 to 0.75, which is in line with the enhanced T_c in $Ba_3Ir_4Ge_{16}$. It is known that λ_{e-ph} is

TABLE I. Keyparameters obtained for $Ba_{n+2}Ir_{4n}Ge_{12n+4}$ (n = 1, 2) superconductors. Three Sommerfeld constants are values estimated from the fitting to low-temperature heat capacity data in two temperature ranges and the theoretical value. The Debye temperatures Θ_D were obtained from low-temperature range and normal-state heat capacities.

		$Ba_3Ir_4Ge_{16}$	$Ba_4Ir_8Ge_{28}$
T_c (K)		6.1	3.2
γ	T_c—10 K	21 (2)	36(3)
(mJ mol^{-1} K^{-2} f.u.$^{-1}$)	T_c—300 K	19(2)	33(2)
	theoretical	31.1	66.2
γ_{atom} (mJ mol^{-1} K^{-2} atom^{-1})		0.91(1)	0.90(1)
$\Delta C/\gamma T_c$		1.85	1.31
	T_c—10 K	240(3)	254(2)
Θ_D (K)	10—300 K	286(4)	303(3)
	T_c—300 K	289(3)	305 (3)
Θ_{E1} (K)		113(1)	118(1)
Θ_{E2} (K)		53(1)	60(1)
λ_{e-ph}		0.75	0.56
shortest Ba-Ge distance	[Ir_8Ge_{16}]	3.596(8)	3.506(2)
(Å)	[Ir_2Ge_{16}]	3.495(2)	3.452(2)
N (E_F) (eV^{-1} f.u.$^{-1}$)		14.4	30.7

proportional to $N(0)/\langle\omega^2\rangle$, where $\langle\omega^2\rangle$ is the average phonon frequency.[23] Considering the enhanced T_c and the reduced $N(0)$ in $Ba_3Ir_4Ge_{16}$, it is evident that the vibration of $\langle\omega^2\rangle$ is significant to account for the higher T_c. As found in previous phonon spectrum calculations on skutterudites[2] and Sr-filled Ge clathrate,[24] the rattler primarily couples with the acoustic phonons of the anion rather than those of transition metal. In the present system, therefore, we propose that the interaction between the additional dispersionless mode and the acoustic phonon of the Ge anion should prevail in the lower-frequency regime of the full phonon spectrum. From the structural analysis, we infer that there is larger vibrational amplitude of the rattler and weaker force constant of Ba-Ge bonds in the bigger cages of $Ba_3Ir_4Ge_{16}$. This expansion of the cage should logically lead to the reduction of Θ_E from 118 K (60 K) to 113 K (53 K). Meanwhile, this softening could reduce the acoustic branches of the full phonon spectrum and then lower the average phonon frequency $\langle\omega^2\rangle$. Simultaneously, it would increase the coupling strength between the rattler and the electron from Ge anions. Since the Ge-4p bands dominate the conductivity and T_c is exponentially increased with λ_{e-ph}, we consider that the enhanced electron-rattler coupling strengthens λ_{e-ph}, which may be responsible for the enhancement of T_c. Certainly, phonon spectrums from both theory and experiment would be highly valuable to confirm it.

IV. SUMMARY

We found the superconductivity in two cage compounds, $Ba_3Ir_4Ge_{16}$ and $Ba_4Ir_8Ge_{28}$, with $T_c = 6.1$ and 3.2 K, respectively. The analysis of normal-state specific heat data demonstrated the presence of a locally low-energy Einstein mode arising from guest Ba atoms. The Debye and characteristic temperatures become smaller due to weaker bonding states between the guest atom and the cage framework, which may be responsible for the enhanced λ_{e-ph} and may favor superconductivity. The perspective of tuning the phonon frequency by controlling the cage size will deepen comprehension of low-energy excitation in three-dimensional cage superconductors or more complex materials.

ACKNOWLEDGMENTS

This Rapid Communication was supported by the Funding Program for World-Leading Innovative Research and Development on Science and Technology, Japan.

*Corresponding author: hosono@msl.titech.ac.jp

[1] V. Keppens, D. Mandrus, B. C. Sales, B. C. Chakoumakos, P. Dai, R. Coldea, M. B. Maple, D. A. Gajewski, E. J. Freeman, and S. Bennington, Nature **395**, 876 (1998).

[2] J. L. Feldman, D. J. Singh, C. Kendziora, D. Mandrus, and B. C. Sales, Phys. Rev. B **68**, 094301 (2003).

[3] B. C. Sales, D. Mandrus, and R. K. Williams, Science **272**, 1325 (1996).

[4] F. M. Grosche, H. Q. Yuan, W. Carrillo-Cabrera, S. Paschen, C. Langhammer, F. Kromer, G. Sparn, M. Baenitz, Y. Grin, and F. Steglich, Phys. Rev. Lett. **87**, 247003 (2001).

[5] Y. Nagao, J. Yamaura, H. Ogusu, Y. Okamoto, and Z. Hiroi, J. Phys. Soc. Jpn. **78**, 064702 (2009).

[6] S. D. Bader, G. S. Knapp, S. K. Sinha, P. Schweiss, and B. Renker, Phys. Rev. Lett. **37**, 344 (1976); F. Y. Fradin, G. S. Knapp, S. D. Bader, G. Cinader, and C. W. Kimball, in *Superconductivity in d- and f-Band Metals*, edited by D. H. Douglass (Plenum Press, New York, 1976), p. 297.

[7] D. J. Safarik, T. Klimczuk, A. Llobet, D. D. Byler, J. C. Lashley, J. R. O'Brien, and N. R. Dilley, Phys. Rev. B **85**, 014103 (2012).

[8] A. Onosaka, Y. Okamoto, J. Yamaura, and Z. Hiroi, J. Phys. Soc. Jpn. **81**, 023703 (2012).

[9] S. Yonezawa, Y. Muraoka, and Z. Hiroi, J. Phys. Soc. Jpn. **73**, 1655 (2004); S. Yonezawa, Y. Muraoka, Y. Matsushita, and Z. Hiroi, *ibid.* **73**, 819 (2004); J. Phys. Condens. Matter **16**, L9 (2004).

[10] H. Mutka, M. M. Koza, M. R. Johnson, Z. Hiroi, J. I. Yamaura, and Y. Nagao, Phys. Rev. B **78**, 104307 (2008).

[11] T. Hasegawa, Y. Takasu, N. Ogita, M. Udagawa, J. I. Yamaura, Y. Nagao, and Z. Hiroi, Phys. Rev. B **77**, 064303 (2008).

[12] J. Yamaura, S. Yonezawa, Y. Muraoka, and Z. Hiroi, J. Solid State Chem. **179**, 336 (2006).

[13] Z. Hiroi, J. Yamaura, and K. Hattori, J. Phys. Soc. Jpn. **81**, 011012 (2012).

[14] TOPAS 2005, version 3 (Bruker AXS, Karlsruhe, Germany).

[15] J. P. Perdew, K. Burke, and M. Ernzerhof, Phys. Rev. Lett. **77**, 3865 (1996); P. E. Blöchl, Phys. Rev. B **50**, 17953 (1994); G. Kresse and J. Furthmüller, *ibid.* **54**, 11169 (1996).

[16] M. Falmbigl, F. Kneidinger, M. Chen, A. Grytsiv, H. Michor, E. Royanian, E. Bauer, H. Effenberger, R. Podloucky, and P. Rogl, Inorg. Chem. **52**, 931 (2013).

[17] See Supplemental Material at http://link.aps.org/supplemental/10.1103/PhysRevB.88.140507 for the Macmillan equation, crystal structure refinement results of PXRD patterns of $Ba_3Ir_4Ge_{16}$, crystallographic parameters of $Ba_4Ir_8Ge_{28}$, synthesis condition and superconductivity of $BaGe_2$, normal-state magnetic susceptibility of $Ba_3Ir_4Ge_{16}$ and $Ba_4Ir_8Ge_{28}$, and detailed DFT calculation results for $Ba_{n+2}Ir_{4n}Ge_{12n+4}$ ($n = 1, 2$).

[18] A. Smakula and J. Kalnajs, Phys. Rev. **99**, 1737 (1955).

[19] E. Bauer, A. Grytsiv, X. Q. Chen, N. Melnychenko-Koblyuk, G. Hilscher, H. Kaldarar, H. Michor, E. Royanian, G. Giester, M. Rotter, R. Podloucky, and P. Rogl, Phys. Rev. Lett. **99**, 217001 (2007).

[20] G. P. Johari, Chem. Phys. **287**, 273 (2003); J. Chem. Phys. **119**, 11912 (2003).

[21] E. Duval, A. Boukenter, and T. Achibat, J. Phys: Condens. Matter **2**, 10227 (1990).

[22] A. I. Chumakov, G. Monaco, A. Monaco, W. A. Crichton, A. Bosak, R. Rüffer, A. Meyer, F. Kargl, L. Comez, D. Fioretto, H. Giefers, S. Roitsch, G. Wortmann, M. H. Manghnani, A. Hushur, Q. Williams, J. Balogh, K. Parliński, P. Jochym, and P. Piekarz, Phys. Rev. Lett. **106**, 225501 (2011).

[23] W. L. McMillan, Phys. Rev. **167**, 331 (1968).

[24] J. Dong, O. F. Sankey, and C. W. Myles, Phys. Rev. Lett. **86**, 2361 (2001).